S1 Uncertainty assessment of EKO ML-020VM Pyranometer measurements

Accuracy of solar radiation measurements from any radiometer depends not only on the specifications of the sensor but also on the calibration procedure, measurement and maintenance protocol, and prevailing environmental conditions. Each of our measurement systems include a pyranometer sensor with an analog-to-digital converter (ADC) data logger and meteorological sensors as described in the instrumentation Sect. 2. Since the present study focuses on the global irradiance and the corresponding transmittance measurements from the pyranometer network, various sources of uncertainty associated with each of these pyranometer sensors is elaborated below.

S1.1 Intrinsic sensor and calibration uncertainties

The uncertainties associated with the measurement sensor and other components of the observing system such as the ADC data logger (including an amplifier) that can influence the measurement signal are combined as intrinsic sensor uncertainty. The relevant parameters of these components associated in the measurement system are mostly available from the manufacturer specifications listed in Table 1. Additionally, the process of calibration involve further uncertainty due to the spectral mismatch of initial reference and transfer sensors.

The global horizontal irradiance (G in $\mathrm{W\,m^{-2}}$) is obtained by using Eq. (1), where the term enclosed in the first parenthesis inside the square bracket denotes the raw signal (V in volts) while the denominator of the fractional term in the second parenthesis denotes the amplification factor (A), and K_c represents the pyranometer responsivity (in $\mathrm{V\,W^{-1}\,m^2}$) determined from the calibration. Eq. 1 can be expressed in a more generalized form as below:

$$G = \left[\frac{V}{A}\right] \cdot \frac{1}{K_c} \tag{S1.1}$$

In our case, the pyranometer sensitivity (K_c) is a sensor-specific constant value determined from the calibration process and is used to convert the raw voltage signal (V) into global irradiance (G) measurements. We assume that there is no thermal offset for EKO silicon photodiode sensors basing on the night time raw data (see Table 1). The variables in Eq. S1.1 are either measured or calculated independently, and are assumed to be uncorrelated.

As the solar spectrum changes with the sun position and variable atmospheric conditions, differences in solar spectra lead to differences on the order of 2 % in global-horizontal irradiance from silicon radiometers (Myers, 2011). If the responsivity was obtained as a function of solar zenith angles, the uncertainty in the responsivity value can be reduced by 50 % (Reda, 1998; Reda et al., 2008). In order to calibrate as a function of solar zenith angle, enormous additional effort is required. Keeping in view of these limitations, we have considered the calibration factors that have been derived independently by the manufacturer in the present study. The calibration factors for our pyranometer sensors varied from 6.71 to 7.67 $\mu\mathrm{V\,W^{-1}\,m^2}$. The mean value of calibration factors was obtained as 7.375 $\mu\mathrm{V\,W^{-1}\,m^2}$ with a standard deviation of 0.22 $\mu\mathrm{V\,W^{-1}\,m^2}$. Since the calibration uncertainties stated by the manufacturer refer to expanded uncertainties obtained by multiplying the corresponding standard uncertainties with a coverage factor (k), the expanded uncertainty (U) in calibration is 0.22 $\mu\mathrm{V\,W^{-1}\,m^2}$ (~ 3 %). This results in a standard uncertainty (u) of 1.5 % (with k = 2). Several other sources of uncertainty that influence the calibration are indicated by the manufacturer (refer Table 1), which include the nonlinearity (<0.2 %), non-stability (± 2 %), temperature response (± 0.5 %), spectral error (± 5 % during the day), and the directional response (1/1.5/17 % for 30°/60°/80°). Here, the 17 % directional response at 80° implies that the sensitivity drops to 0.83 at 80° polar angle of incidence. Though the directional uncertainty is intrinsic to the instrument, depending on the dome and diffuser of the pyranometer, it can be affected by the prevailing operational conditions. The radiance will be isotropic under overcast conditions, and this will reduce the directional uncertainty to almost negligible. On the other hand, if there is a direct sunlight and the sun is low on the horizon, these directional uncertainties will be maximal. Even though these aspects depend on the operational conditions, the directional errors are more pertinent to the sensor and correspond to intrinsic uncertainty. These uncertainties are assumed to exhibit a rectangular distribution, and thus the respective standard uncertainties are obtained by dividing with $\sqrt{3}$ (Reda, 2011). Further,

these are combined with a quadratic sum along with calibration uncertainty to yield a standard uncertainty (u_K) of 3.53–10.4 % (for 30° to 80°), which results in an expanded uncertainty (U_K) of 6.3–18.1 % (for 30° to 80°).

The ADC data acquisition logger system has a gain error of 0.5 % (expanded uncertainty), which results in a standard uncertainty of 0.29 % (u_V) by assuming a rectangular distribution. Similarly, the amplifier has a gain error of 0.3 % (for Gain = 300) resulting in a standard uncertainty of 0.18 % (u_A) with a rectangular distribution.

The sensitivity factors (Taylor and Kuyatt, 1994) of each variable in the measurement equation S1.1 are calculated by obtaining the partial derivatives of global irradiance (G) with respect to the corresponding variable as below:

$$c_K = \frac{\partial G}{\partial K_c} = \frac{-V}{A \cdot K_c^2}, \tag{S1.2}$$

$$c_V = \frac{\partial G}{\partial V} = \frac{1}{A \cdot K_c}, \tag{S1.3}$$

$$c_A = \frac{\partial G}{\partial A} = \frac{-V}{A^2 \cdot K_c}. \tag{S1.4}$$

S1.2 Operational uncertainties

The uncertainties arising from external sources linked to the prevailing operational conditions and the level of maintenance are referred as operational uncertainties (u_{op}). Typical sources of operational uncertainties include soiling of the glass dome, horizontal misalignment of the leveling platform, intercomparison uncertainty, obstructions to free the horizon etc. During the HOPE campaign, a weekly maintenance of each pyranometer station was undertaken to replace the batteries, and a record on the status of cleanliness of glass dome (on a scale of 1-10) and horizontal alignment of the leveling plate (on a scale of 1-3; see Fig. S1) was maintained.

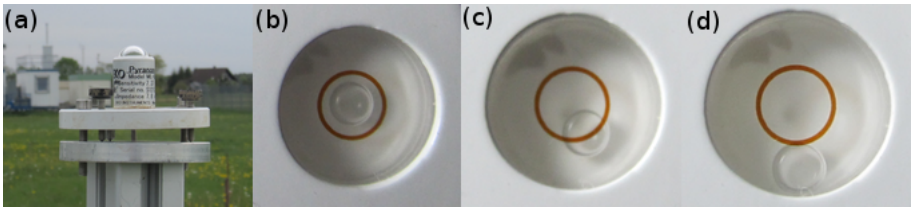

Figure S1. (a) Picture with leveling plate of a pyranometer sensor after perfect horizontal alignment. Possible tilt orientations as seen on the spirit level with the position of the bubble relative to the marked circle: (b) tilt flag = 1, (c) tilt flag = 2, and (d) tilt flag = 3.

S1.2.1 Soiling effects

Soiling of sensors is an important source for underestimation of the measured global irradiances, especially when a daily maintenance is not feasible for a large network of pyranometers. In a study by Al-Alawy (1990), a reduction in transmission between 10 and 40 $\mathrm{W\,m^{-2}}$ per day was observed due to dust deposition in Iraq with no information about its variation with time.

Using Eq. 6, the relative soiling factors (δ_S expressed in absolute units) were obtained for perfectly leveled sensors with instantaneous measurements corresponding to $\pm 5\,\mathrm{min}$ before and after cleaning the sensors during the HOPE campaign. As the frequency of maintenance is on a weekly basis, we cannot accurately assess the dependency on time. So, we represent δ_S as a function of assigned cleanliness flags (2–10) from all available days, irrespective of the prevailing sky condition (Fig. S2). In general, δ_S is supposed to increase with an increase in the assigned cleanliness flags. However, this dependency was not perceived with the observations. This indicates the possible inconsistency while assigning the cleanliness flags due to differences in perception from observer to observer. Further, the observed differences in global irradiance values were scattered with respect to the measurements corresponding to the signal after cleaning. It is possible that the differences in global irradiance between before and after cleaning the glass dome can result in either positive or negative values due the

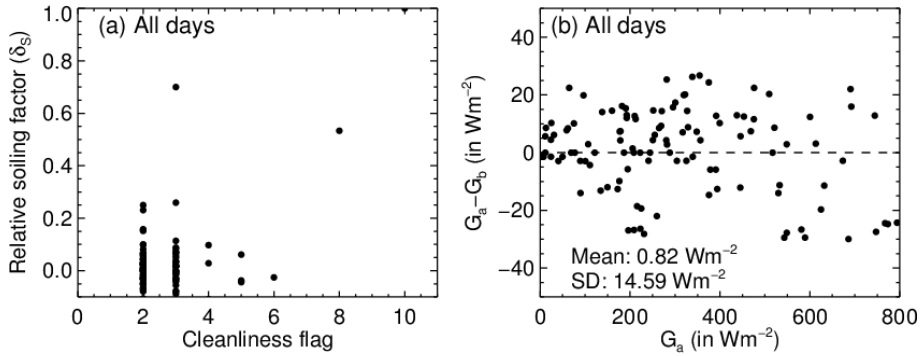

Figure S2. (a) Relative soiling factor (δ_S) as a function of the assigned cleanliness flags, and (b) the change in irradiance signal represented as a function of after clean irradiance measurements from all days of the HOPE campaign. Dashed horizontal black line in (b) represent the zero difference line.

inhomogeneity conditions in the sky and solar geometry. Geuder and Quaschning (2006) presented a method to correct the measured signal influenced by soiling using additional measurements of the direct and diffuse components of irradiance at the same location. They reported that the effect of soiling was more pronounced on pyrheliometers (5 % after 10 days, 5–10 % after 30 days) than on rotating shadowband radiometers (< 5 %). As there exist no separate sensors for measuring other components of irradiance at each measurement station, a similar study is not feasible to derive a constant factor specific to each sensor. Another limitation is the occurrence of rain in between the regular maintenance intervals (~ 1 week) can act as a cleansing agent if it was sufficiently intense. Moreover, the distribution of precipitation cannot be uniform over the entire domain of the pyranometer network. Keeping in view of these and other intricacies, we assume a standard uncertainty of $\pm\, 15\ \mathrm{W\ m^{-2}}$ (from Fig. S2) due to soiling irrespective of our assigned cleanliness flags and the prevailing sky condition.

S1.2.2 Horizontal misalignment errors

In order to quantify the uncertainties associated with the horizontal misalignment of the sensor leveling plate, we have set up three EKO pyranometer stations during the Melpitz-Column experiment at Melpitz, Germany (during 5 May 2015 to 12 May 2015) in three possible tilt orientations of horizontal alignment based on the position of bubble in the spirit-level of the leveling plate: perfect (tilt flag = 1, bubble located within the marked circle), medium (tilt flag = 2, half the bubble located partially in and out of the marked circle) and bad (tilt flag = 3, bubble located completely out of the marked circle) (see Fig. S1).

The dimensionless error factor (δ_T, from Eq. 7) was defined as the ratio of *biased* (due to misalignment, tilt flag = 2 or 3) to the *unbiased* (i.e., perfect horizontal alignment, tilt flag = 1) measurements of global irradiance obtained from the respective EKO pyranometer sensors. This error factor is proportional to both the solar zenith angle (θ_0) and the corresponding angle of deviation due to horizontal misalignment. δ_T (in %) was represented as a function of corresponding solar zenith angles between measurements for tilt flags 1 and 2 (Fig. S3a, b) or 3 (Fig. S3c, d). From figure S3, the relative deviation (δ_T) is almost insensitive to solar position in both cases. While the relative deviation in irradiance obtained between tilt flags 1 and 2 is centered around 0.88 %, the same was shifted to $-\,0.93$ % for the relative deviation observed between tilt flags 1 and 3. As there is no possibility for partitioning of the global irradiance into direct and diffuse components during HOPE, the only option available is to apply a full correction with an assumption that all the downward solar radiation is coming from direct sun. The standard uncertainty due to horizontal misalignment was obtained by considering both the width and the median bias of the percent relative deviation (see Fig. S3). A standard uncertainty of 3.12 % and 3.95 % was resulting due to the tilt flags 2 and 3 (i.e., biased measurement) with respect to the perfectly leveled (i.e., tilt flag 1) unbiased measurement. Further, it is clearly evident that horizontal misalignment has negligible influence on the global irradiance measurements from an EKO pyranometer (see Table 3).

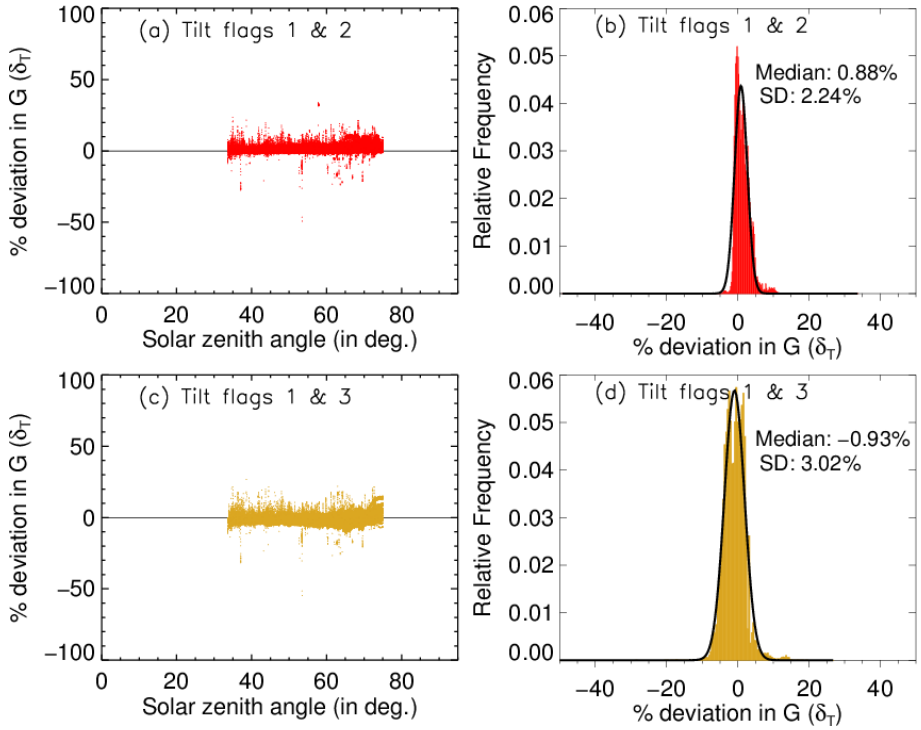

Figure S3. Percentage deviation in global irradiance measurements due to horizontal misalignment of leveling plate as a function of corresponding solar zenith angles obtained for: (a) tilt flags 1 and 2, and (c) tilt flags 1 and 3. Relative frequency distribution of the percentage deviation in global irradiance measurements obtained for (b) tilt flags 1 and 2, and (d) tilt flags 1 and 3. Note that the measurements represented by tilt flag 1 are considered as 'unbiased' whereas those corresponding to either tilt flags 2 or 3 represent the 'biased' measurements.

S1.2.3 Obstructions due to close by structures

Obstruction of direct solar beam due to closely located trees or buildings require correction wherever possible to reduce the uncertainty in the measurements. These are readily detectable on cloudless days, and accurate correction is possible only when both the diffuse and global irradiance measurements are available at each station. Initially, diffuse irradiance (i.e., the fraction of radiation coming from that portion of the sky which is obscured) is corrected and then global irradiance can be adjusted subsequently. It should be noted that contribution of diffuse sky radiation for elevation angles below 5° is less than 1 % and can be neglected.

As an alternate way, we have used the empirical fitting method of (Long and Ackerman, 2000) on global irradiance measurements for clear sky days at each station separately by using a simple power law equation of the form:

$$G = a \cdot (cos\,\theta_0)^b, \tag{S1.5}$$

representing the clear-sky conditions, where G is the clear sky total shortwave irradiance from the pyranometer sensor (in $\mathrm{W\,m^{-2}}$), θ_0 is the solar zenith angle, and a and b are the regression coefficients. An advantage of this Eq. S1.5 is that it models the same physics as that of the prevailing situation. For instance, the constant a represents the clear-sky irradiance for a solar zenith angle of 0° and includes such effects as the average aerosol and column water vapor amounts, the mean Sun-Earth distance on that day, and radiometer calibration. The constant b includes such effects as the radiometer cosine response. The regression coefficients, a and b were determined using a least square robust estimation that minimizes the sum of the absolute

deviations. Here, 'robust' means insensitive to fractionally large departures for a small number of data points from the idealized assumptions of the fit.

Using the above method for clear sky measurements, we found large differences ($\gtrsim 50\,\mathrm{W\,m^{-2}}$) between the clear sky fit model and the actual observations when obstructions were close to pyranometer stations and noticed that these deviations were more pronounced for solar elevation angles until 15°. However, there were around 5 stations whose measurements were influenced for elevation angles greater than 15°. As there were no direct irradiance measurements available at each station, we have limited our data visualization corresponding to the measurements obtained for solar elevation angles greater than 15° (or $\theta_0 < 75°$).

S1.2.4 Intercomparison uncertainty

An intercomparison experiment among our pyranometer sensors (95 nos.) was conducted on 27 March 2013 before deploying to the HOPE Jülich campaign (Fig. S4a). As the prevailing weather conditions were not stable with forecast for snow, the intercomparison was not continued beyond one full day. The relative standard deviation in the measured global irradiance (G) measurements was obtained from the ratio of standard deviation to the corresponding mean. In Fig. S4b, this deviation in G is represented as a function of cosine of solar zenith angles ($49° < \theta_0 < 75°$). The corresponding frequency distribution is shown in Fig. S4c. A linear increase in % deviation of G was observed consistently as solar zenith angle increases with a median deviation around 2 %.

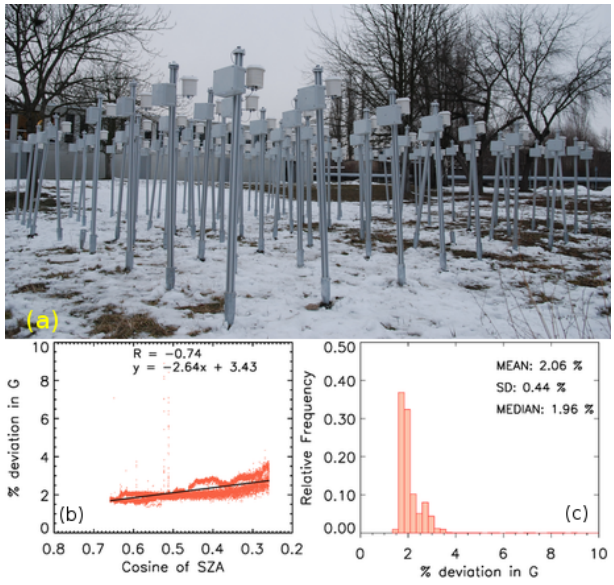

Figure S4. (a) Set up of pyranometer stations (95 nos.) during the intercomparison experiment (on 27 March 2013) at Leipzig, Germany before deployment to the HOPE Jülich campaign. (b) Percent deviation in the global irradiance (G) as a function of the cosine of solar zenith angle (SZA), and (c) corresponding relative frequency distribution of percent deviation in G.

Another intercomparison experiment with 50 pyranometer stations was conducted again during Melpitz-Column experiment at Melpitz, Germany to include more nonhomogeneous sky conditions (Fig. S5). Though the same increasing trend of % relative standard deviation in G was observed with increasing solar zenith angle, the median of the relative standard deviation has increased to 3.0 %. This increase in relative standard deviation of G along with the width of the distribution can be attributed to the differences in direct and diffuse components under variable sky conditions.

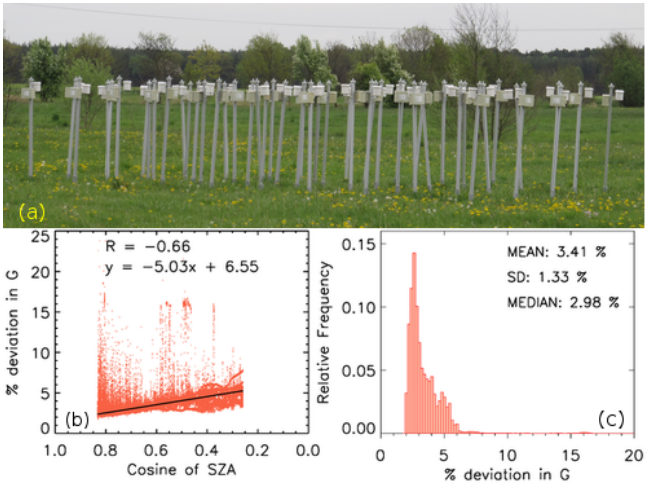

Figure S5. (a) Set up of pyranometer stations (50 nos.) during the intercomparison experiment (from 5 May 2015 to 12 May 2015) at Melpitz, Germany. (b) Percent deviation in shortwave global irradiance (G) as a function of cosine of solar zenith angle (SZA), and (c) corresponding relative frequency distribution of percent deviation in G.

S1.3 Combined uncertainty estimation

By averaging the 10 Hz measurements of global irradiance (G) to corresponding 1 Hz data sets, a standard uncertainty of $< 4\,\mathrm{W\,m^{-2}}$ (i.e., u_{stat}) was observed with a normal distribution under all sky conditions. All the sources contributing to the uncertainty in the global irradiance (G) measurements were listed in Table S1.

Global transmittance (T) is derived from the measured global irradiance (G) measurements through Eq. 5 and this can be expressed in a more simplified form as below:

$$T = \frac{G}{S_0 \cdot \cos\theta_0}. \tag{S1.6}$$

Here, S_0 represents the climate significant total solar irradiance value ($= 1360.8 \pm 0.5\,\mathrm{W\,m^{-2}}$) obtained from Kopp and Lean (2011), and $\cos\theta_0$ denote the cosine of solar zenith angle (θ_0). Though the equations from Liou (2002) were used in the computation of solar coordinates, there may be an uncertainty in θ_0 calculation. So, an expanded uncertainty of 0.05° was assumed in the resulting θ_0 calculations (i.e., u_{th} = 0.025°). The sensitivity coefficients corresponding to G, S_0 and θ_0 are denoted by c_G, c_S and c_{th} respectively. These are obtained with the following equations:

$$c_G = \frac{\partial T}{\partial G} = \frac{1}{S_0 \cdot \cos\theta_0}, \tag{S1.7}$$

$$c_S = \frac{\partial T}{\partial S_0} = \frac{-G}{S_0^2 \cdot \cos\theta_0}, \tag{S1.8}$$

$$c_{th} = \frac{\partial T}{\partial \theta_0} = \frac{G \cdot \tan\theta_0}{S_0 \cdot \cos\theta_0}. \tag{S1.9}$$

The combined standard uncertainty in global transmittance (u_T) can be obtained from the following equation:

$$u_T = \sqrt{c_G^2 \cdot u_G^2 + c_S^2 \cdot u_S^2 + c_{th}^2 \cdot u_{th}^2}, \tag{S1.10}$$

where u_G, u_S and u_{th} correspond to the standard uncertainties of the global irradiance (G), total irradiance at the TOA (S_0), and solar zenith angle (θ_0). Assuming K_c = 7.375 $\mu\mathrm{V\,W^{-1}\,m^2}$ and A = 300, we have calculated the sensitivity coefficients

Table S1. Contributions to uncertainties affecting shortwave global horizontal irradiance (G) and corresponding derived transmittance (T) measurements from an EKO ML-020VM pyranometer.

Uncertainty component	Parameter	Statistical distribution	Standard uncertainty (u_i)	Expanded uncertainty (U_i)
Sensitivity factor				
Calibration	K_c	Normal[a]	1.5 %	3.0 %
Non-stability	K_c	Rectangular[b]	1.15 %	2.0 %
Non-linearity	K_c	Rectangular	0.12 %	0.2 %
Temperature response	K_c	Rectangular	0.29 %	0.5 %
Spectral error	K_c	Rectangular	2.9 %	5.0 %
Directional response (30°–80°)	K_c	Rectangular	0.6–9.8 %	1–17 %
Data acquisition system				
Gain error	V	Rectangular	0.29 %	0.5 %
Amplifier				
Gain error (for Gain=300)	A	Rectangular	0.18 %	0.3 %
Operational uncertainties				
Soiling				
Soil flags = 2-10	G	Normal	15 $\mathrm{W\,m^{-2}}$	30 $\mathrm{W\,m^{-2}}$
Leveling				
Tilt flag = 2	G	Normal	3.12 %	6.24 %
Tilt flag = 3	G	Normal	3.95 %	7.90 %
Inter-comparison uncertainty				
EKO photodiode sensors	G	Normal	2.5 %	5.0 %
Statistical uncertainty				
Conversion of 10 Hz to 1 Hz resolution data	G	Normal	4.0 $\mathrm{W\,m^{-2}}$	8.0 $\mathrm{W\,m^{-2}}$
Additional uncertainties (for transmittance)				
Solar zenith angle	T	Normal	0.025°	0.05°
Extraterrestrial irradiance	T	Normal	0.25 $\mathrm{W\,m^{-2}}$	0.5 $\mathrm{W\,m^{-2}}$

[a] For a normal distribution, the standard uncertainty (u_i) is given by $\frac{U_i}{2}$.
[b] For a rectangular distribution, the standard uncertainty (u_i) is given by $\frac{U_i}{\sqrt{3}}$.

for small (G = 50 $\mathrm{W\,m^{-2}}$) and large (G = 1000 $\mathrm{W\,m^{-2}}$) signals using the Eqs. S1.2 to S1.4 and S1.7 to S1.9. The sensitivity coefficients for different variable parameters were included in Table S2 along with other operational (u_{op}) and statistical (u_{stat}) uncertainties. Assuming that there were no operational uncertainties ($u_{op} = 0$), the combined standard uncertainty of G (u_G) was obtained as 4.4–6.6 $\mathrm{W\,m^{-2}}$ (at 30°–80° polar angles of incidence) for small signal and 35.5–104.5 $\mathrm{W\,m^{-2}}$ (at 30°–80° polar angles of incidence) for large signal. The expanded uncertainties with 95% confidence level were computed by multiplying the obtained standard uncertainties (u_i) with a coverage factor (k=1.96) corresponding to infinite degrees of freedom. For different cases, the standard (u_i) and expanded (U_i) uncertainties were listed in Table 3 for both global irradiance (G) and the corresponding derived transmittance (T) measurements using an EKO photodiode pyranometer. Large signals at 80° polar angles of incidence induce larger uncertainties but in reality such a case doesn't exist. However, these are included to ascertain the limits of possible uncertainty for an EKO ML-020VM pyranometer sensor due to directional errors.

Table S2. Sensitivity factors and combined standard uncertainty contributions due to various sources influencing the measurements of global irradiance (G) and corresponding derived global transmittance (T).

Variable (i)	Standard uncertainty (u_i)		Sensitivity factor (c_i)		$c_i^2 u_i^2$	
	Small[a]	Large[b]	Small	Large	Small	Large
Sensitivity (K_c)	$\mu VW^{-1}m^2$	$\mu VW^{-1}m^2$	$\mu V^{-1}W^2m^{-4}$	$\mu V^{-1}W^2m^{-4}$	W^2m^{-4}	W^2m^{-4}
(at 30° & 80° angles of incidence)	0.26 − 0.77	0.26 − 0.77	6.8	135.6	3.13 − 27.4	0.124−1.09 ($\times 10^4$)
Raw voltage (V)	mV	mV	$mV^{-1}\,Wm^{-2}$	$mV^{-1}\,Wm^{-2}$		
	0.58	0.021	0.452	0.452	0.069	0.00009
Amplification (A)			Wm^{-2}	Wm^{-2}		
	0.54	0.54	0.167	3.333	0.0081	3.24
Operational uncertainties (op)	Wm^{-2}	Wm^{-2}				
Soiling	15	15	–	–	225.0	225.0
Leveling: Tilt flags = 1 & 2	1.56	31.2	–	–	2.43	973.44
Leveling: Tilt flags = 1 & 3	1.98	39.5	–	–	3.90	1560.25
Inter-comparison uncertainty	1.25	25.0	–	–	1.56	625.0
Statistical uncertainty (stat)	Wm^{-2}	Wm^{-2}				
Conversion of 10 Hz to 1 Hz resolution data	4.0	4.0	–	–	16.0	16.0
Additional uncertainties	Wm^{-2}	Wm^{-2}	$W^{-1}m^2$	$W^{-1}m^2$		
Global irradiance (u_G)	u_G	u_G	0.000735	0.000735		
Solar zenith angle (u_{th})	1.0	1.0	3.2×10^{-6}	0.64×10^{-6}	104.9×10^{-12}	0.168×10^{-12}
Extraterrestrial irradiance (u_S)	0.25 Wm^{-2}	0.25 Wm^{-2}	2.7×10^{-5}	5.4×10^{-4}	4.6×10^{-11}	1.8×10^{-8}

[a] Small signal correspond to 50 Wm^{-2} of global horizontal irradiance (G).
[b] Large signal correspond to 1000 Wm^{-2} of global horizontal irradiance (G).

References

Al-Alawy, I. T.: Wind and other factor requirements to solar energy applications in Iraq, Solar and Wind Technology, 7(5), 597–600, 1990.

Geuder, N. and Quaschning, V.: Soiling of irradiance sensors and methods for soiling correction, Solar Energy, 80, 1402–1409, doi:10.1016/j.solener.2006.06.001, 2006.

Kopp, G. and Lean, J. L.: A new, lower value of total solar irradiance: Evidence and climate significance, Geophys. Res. Lett., 38, L01706, doi:, 2011.

Liou, K. N.: An Introduction to Atmospheric Radiation, vol. 84 of International Geophysics Series, Academic Press, USA, second edn., 2002.

Long, C. N. and Ackerman, T. P.: Identification of clear skies from broadband pyranometer measurements and calculation of downwelling shortwave cloud effects, J. Geophys. Res., 105, 15609–15626, doi:10.1029/2009JD900077, 2000.

Myers, D. R.: Quantitative Analysis of Spectral Impacts on Silicon Photodiode Radiometers, in: SOLAR 2011, NREL/CP-5500-50936, Raleigh, North Carolina, http://www.nrel.gov/docs/fy11osti/50936.pdf, last access: 12 January 2016, 2011.

Reda, I.: Improving the accuracy of using pyranometers to measure the clear sky global solar irradiance, Tech. Rep. TP-560-24833, NREL, 1998.

Reda, I., Myers, D. R. and Stoffel, T. L.: Uncertainty estimate for the outdoor calibration of Solar Pyranometers: A metrologist perspective, The Journal of Measurement Science, 3(4), 58–66, 2008.

Reda, I.: Method to Calculate Uncertainties in Measuring Shortwave Solar Irradiance Using Thermopile and Semiconductor Solar Radiometers, NREL, CO, USA, 2011.

Taylor, B. N. and Kuyatt, C. K.: Guidelines for Evaluating and Expressing the Uncertainty of NIST measurement results, Tech. Rep. NIST Technical Note 1297, NIST, 1994.